A Comparative Study on the Various Blocking Layers for Performance Improvement of Dye-sensitized Solar Cells

Jong-Su Woo and Gun-Eik Jang[†]
Department of Advanced Materials Engineering, Chungbuk National University, Cheongju 361-763, Korea

In this study, short-circuit preventive layer (blocking layer) was deposited between conductive transparent electrode and porous TiO_2 film in the DSSCs. As blocking layer, we selected the metal-oxide such as TiO_2, Nb_2O_5 and ZnO. The sheet resistance with each different blocking layers were 18 Ω/sq. for the TiO_2, 10 Ω/sq. for the Nb_2O_5 and 8 Ω/sq. for the ZnO, while the RMS (Root Mean Square) roughness value of DSSCs were 39.61 nm for the TiO_2, 41.84 nm for the Nb_2O_5 and 36.14 nm for the ZnO respectively. From the results of photocurrent-voltage curves, a sputtered Nb_2O_5 blocking layer showed higher performance on 2.64% of photo-electrochemical properties. The maximum of conversion efficiency which was achieved under 1 sun irradiation by depositing the blocking layer increased up to 0.56%.

1. INTRODUCTION

Dye-sensitized solar cells (DSSCs) are promising alternative to the conventional p-n junction solar cells [1], due to simple structure and process, low cost fabrication, transparency, color control, and applicability in the flexible DSSCs [2-4]. The DSSCs are composed of a dye-adsorbed nano-porous TiO_2 layer on fluorine-doped tin oxide (FTO) electrode, redox electrolytes and the counter electrode [5].

To generate meaningful electrical power from DSSCs, the electrons need to pass four important interfaces of DSSCs: dye/TiO_2, TiO_2/FTO, electrolyte/counter electrode, and dye/electrolyte [6]. As the key component of DSSCs, the nano-porous TiO_2 electrode shows high surface area, which enables both efficient electron injection and light harvesting [7].

However, it also provides abundant TiO_2 surface sites (direct route) and bare FTO conducting sites (indirect route), where the photo injected electrons may recombine with I3- species in the
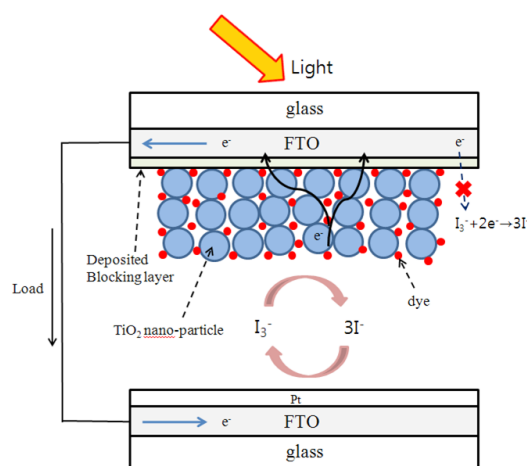

Fig. 1. Schematic view of interfaces in the DSSCs device.

redox electrolyte ($2e^- + I_3^- \rightarrow 3I^-$) [8-10].

The charge recombination mainly occurs at the electrode/electrolyte interface due to the absence of energy barrier layer [11,12]. The recombination will cause the loss of the photocurrent. So the photovoltaic performance of DSSCs is seriously

[†] Author to whom all correspondence should be addressed:
E-mail: gejang@chungbuk.ac.kr

Trans. Electr. Electron. Mater. 14(6) 312 (2013): J.-S. Woo *et al.*

313

decreased [13]. Recently, the charge recombination can be significantly suppressed by employing a thin blocking layer [14,15] as shown in Fig. 1. Semiconductors, such as TiO_2, Nb_2O_5, ZnO and some insulating materials, such as $CaCO_3$ and $BaCO_3$, have been used as a blocking layer for the fabrication of DSSCs [16-20].

In this work, we systematically investigated and compared the optical, structural, and photo- electrochemical properties based on different types of blocking layers such as TiO_2, Nb_2O_5, and ZnO. We expected that the electrodeposited various blocking layers (TiO_2, Nb_2O_5 and ZnO) at the exposed TiO_2/FTO interface contributes to the suppression of the charge recombination.

2. EXPERIMENTS

2.1 Preparation of the standard DSSC

The FTO glasses (7 Ω/sq.) that we used were cleaned thoroughly in acetone and ethanol for 30 min in each step to remove the organic pollutants and other contamination [21]. After drying by Ar compressed gas, TiO_2 nano-particle paste was coated on the FTO electrode by using the doctor-blade technique. And then TiO_2 nano-porous film was annealed at 500℃ for 30 min in air. The thickness of TiO_2 film was approximately 14 μm. Ru complex dye (N719; 535 bis-TBA : cis-bis (isothiocyanato) and bis (2, 2'-bipyridyl-4, 4'-dicarboxylato) -ruthenium(Ⅱ) bis-tetrabutylammonium 0.05 g in 100 ml absolute ethanol (99.99%)) was synthesized in advance. To adsorb a photo sensitized dye on the TiO_2 surface the TiO_2 working electrode was immersed in Ru complex dye (N719) for 24 h at room temperature. Immediately the dye-adsorbed TiO_2 working electrode was rinsed with absolute ethanol and dried by Ar compressed gas. The counter electrode was prepared by sputtering (sputter coater; sc 7640) a pt layer on the other FTO coated glass electrode. The Pt-treated electrode was placed over the dye-coated electrode and edges of the cell were sealed with 0.5 mm wide strips of 60 μm-thick surlyn (solarnix, sx 1170, Hot Met). After sealing, an iodide based electrolyte of tri-iodide in acetonitrile (solarnix, AN-50) was injected into the cell through of the two small holes drilled in the counter electrode. The holes were then covered with small cover glass and sealed.

2.2 Preparation of the added blocking layer (TiO_2, Nb_2O_5 and ZnO) to DSSC

As the blocking layer materials, TiO_2, Nb_2O_5 and ZnO were selected in this study. The blocking layer was deposited between the FTO glass and TiO_2 nano-porous film by using RF magnetron sputter. The TiO_2, Nb_2O_5 and ZnO ceramic targets were fabricated (diameter; 2 inch) with high purity TiO_2 (99.99%), Nb_2O_5 (99.99%) and ZnO (99.99%) powders respectively. More details about the sputtering conditions are given in Table 1.

The deposition conditions were maintained carefully stable during the growth of blocking layer. After that, those were fabricated in the same way as the standard DSSCs.

2.3 Measurements

The film thickness were measured using a surface profilier meter (α-step, TENCOR P-2). The crystal structure of the film was analyzed by x-ray diffractometer (XRD; Rigku). The film morphology was observed by field emission scanning electron microscope (FE-SEM; JEOL). The electrical resistivity of the film was obtained using a four-point probe method. The Model name

Table 1. The fabrication of different blocking layers using RF magnetron sputtering method.

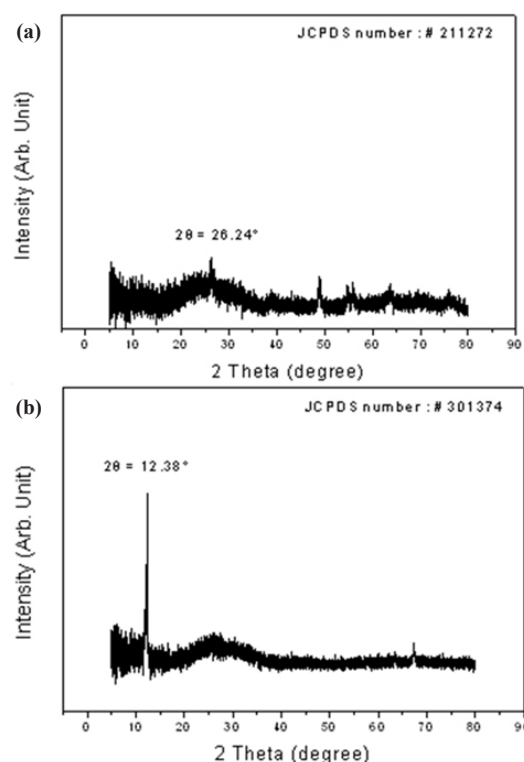| Target	TiO_2	ZnO	Nb_2O_5
electrode temperature	500℃	500℃	500℃
target-electrode distance	55 mm	55 mm	55 mm
atmosphere gas (Ar)	50 sccm	50 sccm	50 sccm
base pressure	1.4×10^{-5} Torr	1.4×10^{-5} Torr	1.4×10^{-5} Torr
working pressure	1.7×10^{-2} Torr	1.7×10^{-2} Torr	1.7×10^{-2} Torr
RF power	100 W	100 W	100 W

Fig. 2. XRD patterns of (a) TiO_2 nano-porous film and (b) FTO electrode annealed at 500℃ electrode temperature.

of Nanoscope Ⅲa was used to perform atomic force microscopic (AFM) studies. The photocurrent-voltage (I-V) characteristics of the DSSCs were measured under AM 1.5, 100 mW/m^2 (1 sun) using a solar simulator.

3. RESULTS AND DISCUSSION

Figure 2 showed the XRD patterns of TiO_2 nano-porous film and FTO electrode annealed at 500℃ electrode temperature.

In case of the Fig. 2(a), due to the background's peaks it seems like amorphous phase. But it clearly represented tendency of the crystallinity in TiO_2 nano-porous film with (101) preferred orientation at 2 θ = 32.196°. The TiO_2 nano-porous film exhibited TiO_2 anatase crystalline phase. Fig. 2(b) showed XRD patterns of FTO electrode annealed at 500℃ electrode temperature.

The FTO electrode showed the tendency of the crystallinity with (110) prefered orientation at 2 θ = 12.38°. It believed that the FTO electrode has excellent thermal stability because high temperature does not change the crystallity of FTO electrode.
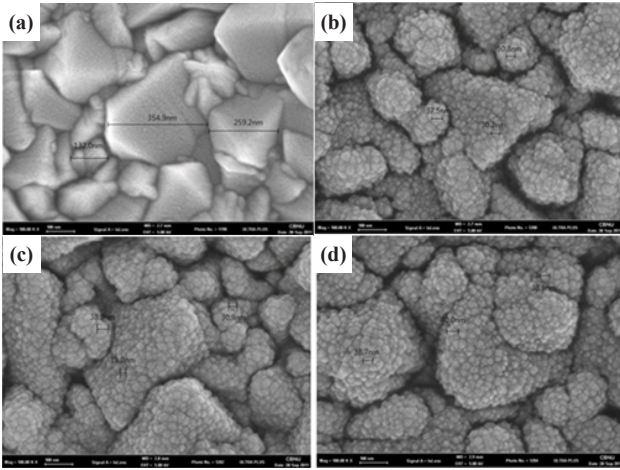
Fig. 3. Surface SEM images of (a) bare FTO electrode, (b) TiO$_2$ deposited FTO selectrode, (c) Nb$_2$O$_5$ deposited FTO electrode, and (d) ZnO deposited FTO electrode.

Fig. 5. Cross sectional SEM images of (a) bare FTO electrode, (b) TiO$_2$ deposited FTO electrode, (c) Nb$_2$O$_5$ deposited FTO electrode, and (d) ZnO deposited FTO electrode.
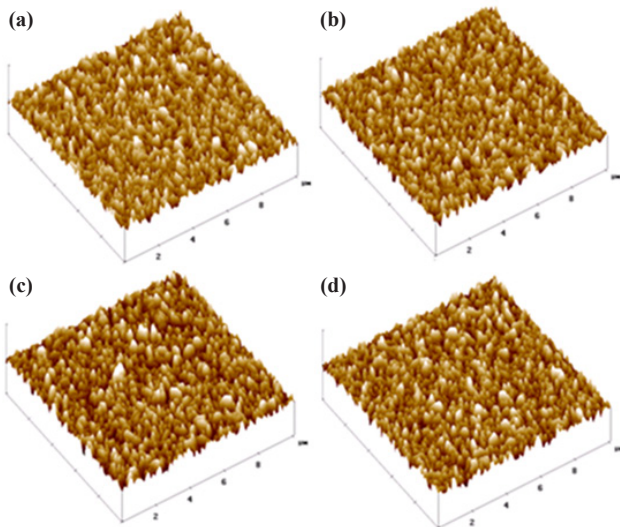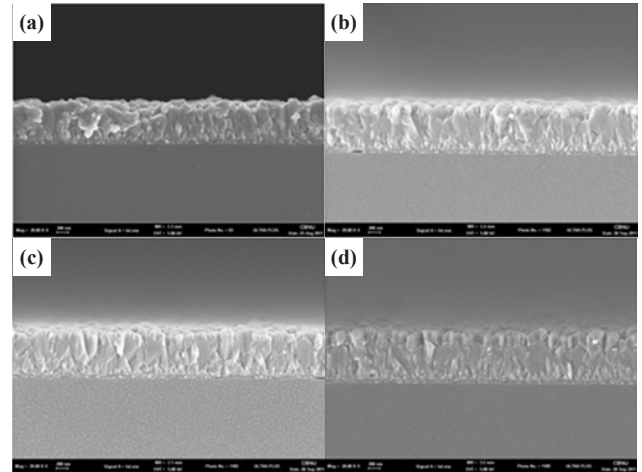

Fig. 4. Three-dimensional AFM images of (a) bare FTO electrode, (b) TiO$_2$ deposited FTO electrode, (c) Nb$_2$O$_5$ deposited FTO electrode, and (d) ZnO deposited FTO electrode.
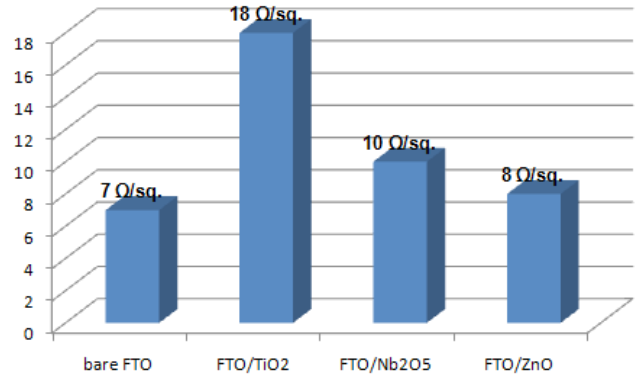

Fig. 6. Sheet resistance of (a) bare FTO electrode, (b) TiO$_2$ deposited FTO electrode, (c) Nb$_2$O$_5$ deposited FTO electrode, and (d) ZnO deposited FTO electrode.

From the XRD results, it is clear that the structure of the fim such as TiO$_2$ nano-porous film and FTO electrode are completely crystalline phase by annealing at 500℃.

Figure 3 and Fig. 4 showed the FE-SEM and AFM images of bare FTO and sputtered blocking layers such as TiO$_2$, Nb$_2$O$_5$ and ZnO on the FTO glass.

From the AFM images, it is clear that the sputtered blocking layers have smooth surface with RMS roughness value which decreased by ~7 nm.

The surface roughness is one of the important factors that determined optical properties. The thin film with flat and low surface roughness value shows a low reflectivity because the constructive interference and destructive interference are clearer according to the thickness.

From FE-SEM images, bare FTO showed the texture surface morphology which has diameter above 1 μm. In case of blocking layers deposited FTO electrodes in Fig. 3(b), Fig. 3(c) and Fig. 3(d) showed that TiO$_2$, Nb$_2$O$_5$ and ZnO nano-particles were covered on the FTO electrode respectively. It is clear that the block-

ing layers which have diameter up to 40 nm were deposited on FTO glass.

Figure 5 showed the cross sectional SEM images of bare FTO and various blocking layer deposited FTO electrodes. As the thickness of the TiO$_2$ nano-porous film is above 14 μm, the images was not shown the material interface clearly. However, before sputtering the blocking layers, we calculated the deposition rate under the same condition. So, we are confident that the thickness of blocking layers are deposited approximately 50 nm even if the SEM images does not shown the thickness clearly. And also, in case of FE-SEM images in Fig. 3, it is clear that the difference from bare FTO was seen. It means that the blocking layers were deposited on FTO glass. It could be confirmed that TiO$_2$, Nb$_2$O$_5$ and ZnO blocking layers are approximately 50 nm respectively.

Figure 6 showed the sheet resistance of bare FTO electrode and blocking layers of TiO$_2$, Nb$_2$O$_5$ and ZnO sputtered on FTO electrode.

The sheet resistance of bare FTO electrode was about 7 Ω/sq. However, after deposited the blocking layers on FTO electrodes, the sheet resistances were obtained such as FTO/TiO$_2$ = 18 Ω/sq., FTO/Nb$_2$O$_5$ = 10 Ω/sq., FTO/ZnO = 8 Ω/sq. respectively.

Especially, the most increased value of sheet resistance was obtained from TiO$_2$ deposited FTO electrode. These results, we

Trans. Electr. Electron. Mater. 14(6) 312 (2013): J.-S. Woo *et al.*

315

expected that the TiO$_2$ deposited FTO electrode will negatively affect the current density (J$_{sc}$) and the conversion efficiency (η).

Figure 7 showed the photocurrent density-voltage (J-V) curves obtained under 100 mW/m^2 illumination with AM 1.5 conditions of DSSCs consisting of TiO$_2$ electrode without and with blocking layer of TiO$_2$, Nb$_2$O$_5$ and ZnO.

The characteristic parameters for DSSCs can be obtained from the photocurrent density-voltage curve, such as the short circuit current (J$_{sc}$), the open circuit voltage (V$_{oc}$), fill factor (FF) and conversion efficiency (η).

The efficiency η of the DSSCs can be calculated from the following equation;

$$\eta = J_{sc} V_{oc} FF / Pin \tag{1}$$

where, J$_{sc}$ is the integral photocurrent density(current obtained at short circuit conditions divided by the area of the cell), V$_{oc}$ is the open circuit voltage, FF is the fill factor, FF = (I × V)max/I$_{sc}$V$_{oc}$ (related to the serious resistance for a potential solar cells), and P$_{in}$ is the intensity of the incident light.

The characteristic parameters for the DSSCs corresponding to Fig. 7 are summarized in Table 2. The DSSC fabricated on the bare FTO/glass electrode showed V$_{oc}$ of 0.6846 V, J$_{sc}$ of 4.0175 mA/cm^2, FF of 75.9849, and calculated power conversion efficiency of η$_{AM1.5}$ = 2.08%. The DSSC deposited with Nb$_2$O$_5$ blocking layer, showed maximum efficiency. As compared with standard DSSC, the conversion efficiency (η), short circuit current (J$_{sc}$) of the DSSC with the Nb$_2$O$_5$ blocking layer were improved in 26.9% and 35.5% respectively. On the other hand, the open circuit voltage (V$_{oc}$) was slightly diminished by 1.6%. Another feature seen in this figure, the DSSCs with the TiO$_2$ and ZnO blocking layers showed the also enhanced efficiency, η (2.24%), η (2.64%) and short circuit current, J$_{sc}$ (4.2048 mA/cm^2), J$_{sc}$ (4.6245 mA/cm^2) respectively.

The reason for the enhancement of J$_{sc}$ with blocking layer is associated with the result of increase of protection effect against ionic penetration from electrolyte through the blocking layer. Consequently, the cell performance under illumination seems to indicate a decrease of the recombination rate in the cell when TiO$_2$, Nb$_2$O$_5$ and ZnO were used as the blocking layer.

However, the DSSC with the TiO$_2$ blocking layer showed lower efficiency than DSSCs with the Nb$_2$O$_5$ and ZnO blocking layer. The lower efficiency of DSSC with the TiO$_2$ blocking layer possibly attributed to the fact of increment of the sheet resistance. As mentioned earlier, the sheet resistance value of FTO/TiO$_2$ electrode is more than twice larger than the sheet resistance values of Nb$_2$O$_5$ and ZnO. For this reason, we considered that short circuit current, J$_{sc}$ was electronically lower than those of Nb$_2$O$_5$ and ZnO. Also we might infer that TiO$_2$, Nb$_2$O$_5$, and ZnO deposited on FTO electrodes were effectively reduce the electron recombination by minimizing the direct contact between the redox electrolyte and the conductive FTO surface.

4. CONCLUSIONS

In summary, the characteristics of the RF sputter grown various blocking layers (TiO$_2$, Nb$_2$O$_5$ and ZnO) on the FTO electrode were investigated for the possible application of DSSCs. The DSSC deposited with Nb$_2$O$_5$ blocking layer, showed maximum efficiency. Compared with standard DSSC, the conversion efficiency (η), short circuit current (J$_{sc}$) of the DSSC with the Nb$_2$O$_5$ blocking layer were improved in 26.9% and 35.5% respectively. On the other hand, the open circuit voltage (V$_{oc}$) was slightly

Table 2. The fabrication of different blocking layers using RF magnetron sputtering method.

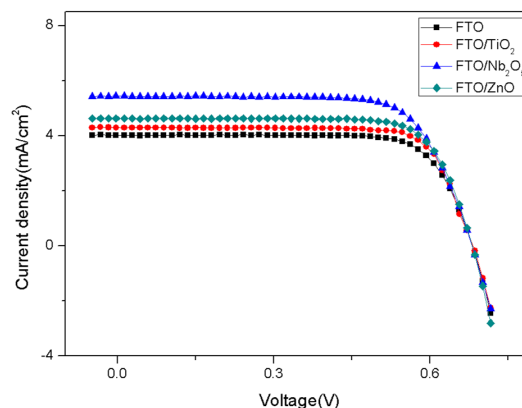|	V$_{oc}$ (V)	J$_{sc}$ (mA/cm^2)	FF	η (%)
Bare FTO	0.68	4.01	75.98	2.08
FTO/TiO$_2$	0.69	3.09	76.27	1.64
FTO/Nb$_2$O$_5$	0.67	5.44	71.96	2.64
FTO/ZnO	0.68	4.62	75.76	2.38

Fig. 7. Photocurrent-voltage curves with different types of blocking layer; (a) bare FTO electrode, (b) TiO$_2$, (c) Nb$_2$O$_5$, and (d) ZnO.

diminished by 1.6%. Among the DSSCs with the blocking layers, the DSSCs with the TiO$_2$ blocking layer showed lower efficiency than DSSCs with the Nb$_2$O$_5$ and ZnO blocking layers.

REFERENCES

[1] B. O'Regan, M. Gräzel, Nature (London) 353 (1991) 737.
[2] M. Grätzel, Dye-sensitised solar cells: review, J. Photochem. Photobiol. C:
[3] A. F. Nogueira, C.L ongo, M.-A. Depaoli, Polymers in dye sensitized cells: overview and perspectives: review, Coord. Chem. Rev. 248 (2004) 1455-1468. D. L. Eaten, US Patent **3**, 904 422 (1975).
[4] B.A. Gregg, Interfacial processes in the dye-sensitized solar cell: review, Coord. Chem. Rev. 248 (2004) 1215-1224.
[5] M.F. Hossain, S. Biswas, T. Takahashi. Thin Solid Films 517 (2008) 1294-1300
[6] H. You, S. Zhang, H. Zhao, G. Will, P. Liu, Electochimica Acta 54 (2009) 1319-1324
[7] S. W, H. HAN, Q. Tai, J. Zhang, S. Xu, C. Zhou, Y. Yang, H. Hu, B. Chen, X.Z. Zhao, Journal of Power Souces 182 (2008) 119-123.
[8] J.R. Durrant, S.A. Haque, E. Palomares, Coord. Chem. Rev. 248 (2004) 1247.
[9] P. J. Cameron, L. M. Peter, J. Phys. Chem. B 107 (2003) 14394.
[10] K. Kalyanasundaram, M. Gratzel, Coord. Chem. Rev. 177 (1998) 347.
[11] E. Palmares, J. N. Clifford, S. A. Haque, T. Lutz, J.R. Durrant, Chem. Commun. (2002) 1464-1465.
[12] Z.-S. Wang, M. Yanagida, K. Sayama, H. Sugihara, Chem. Mater.

18 (2006) 2912-2916.

[13] E. Palomares, J.N. Clifford, S.A. Haque, T. Lutz, J.R. Durrant, J. Am. Chem. Soc. 125 (2003) 475-482.

[14] P. J. Cameron, L. M. Peter, S. Hore, J. Phys. Chem. B 109 (2005) 930.

[15] S. Ito, P. Liska, P. Comte, R. Charvet, P. Pèhy, U. Bach, L. Schmidt-Mende, S. M. Zakeeruddin, A. Kay, M. K. Nazeeruddin, M. Gräzel, Chem. Commun. (2005) 4351.

[16] J. N. Hart, D. Menzies, Y.-B. Cheng, G. P. Simon, L. Spiccia, C. R. Chim. 9 (2006) 622.

[17] J. Xia, N. Masaki, K. Jiang, S. Yanagida, J. Phys. Chem. C 111 (2007) 8092.

[18] S.-J. Roh, R. S. Mane, S.-K. Min, W.-J. Lee, C. D. Lokhande, S.-H. Han, Appl. Phys. Lett. 89 (2006), 253512/1.

[19] Z.-S.Wang, M. Yanagida, K. Sayama, H. Sugihara, Chem. Mater. 18 (2006) 2912.

[20] X.Wu, L.Wang, F. Luo, B. Ma, C. Zhan, Y. Qiu, J. Phys. Chem. C 111 (2007) 8075.

[21] S.U. Lee, W.S. Choi, Byungyou Hong, Sol. Ener. Mater & sol. Cel. 94 (2010) 680-685.